Deformation of accretionary wedges in response to seamount subduction: Insights from sandbox experiments

S Dominguez, J Malavieille, Serge E. Lallemand

TECTONICS, VOL. 19, NO. 1, PAGES 182-196 FEBRUARY 2000

Deformation of accretionary wedges in response to seamount subduction: Insights from sandbox experiments

S. Dominguez, J. Malavieille, and S. E. Lallemand

Laboratoire de Géophysique, Tectonique et Sédimentologie, UMR 5573, CNRS
Institut des Sciences de la Terre, de l'Eau et de l'Espace de Montpellier
Université de Montpellier II, Montpellier, France

Abstract. Sandbox experiments, using a two-dimensional and a three-dimensional approach, are used to study the deformation of margins in response to seamount subduction. Successive mechanisms of deformation are activated during the subduction of conical seamounts. First, reactivation of the frontal thrusts and compaction of the accretionary wedge is observed. Then, back thrusting and, conjugate strike-slip faulting develops above the leading slope of the subducted seamount. The basal décollement is deflected upward in the wake of the subducting high, and a large shadow zone develops behind the seamount trailing slope. Consequently, frontal accretion is inhibited and part of the frontal margin is dragged into the subduction zone. When the main décollement returns to its basal level in the wake of the seamount, the margin records a rapid subsidence and a new accretionary wedge develops, closing the margin reentrant. The sediments underthrusted in the wake of the seamount into the shadow zone, are underplated beneath the rear part of the accretionary wedge. Substantial shortening and thickening of the deformable seaward termination of the upper plate basement, associated with basal erosion is observed. Seamount subduction induces significant material transfer within the accretionary wedge, favors large tectonic erosion of the frontal margin and thickening of the rear part of the margin. The subduction and underplating of relatively undeformed, water-ladden sediments, associated with fluid expulsion along the fractures affecting the margin could modify the fluid pressure along the basal décollement. Consequently, significant variations of the effective basal friction and local mechanical coupling between the two plates could be expected around the subducting seamount.

1. Introduction

1.1. Geologic Setting

Large domains of oceanic plates (Figure 1) are characterized by a very rough seafloor covered by numerous seamounts, aseismic ridges, and volcanic plateaus [*Batiza*, 1982; *Smith and Jordan*, 1988; *Wessel and Lyons*, 1997]. As revealed by marine data and large-scale observations [*Ballance et al.*, 1989; *Collot and Fisher*, 1989, 1991; *Fisher et al.*, 1991; Lallemand *et al.*, 1990; *von Huene and Scholl*, 1991; *von Huene et al.*, 1995; *Moore and Sender*, 1995; *Dominguez et al.*, 1998, 1999; Park et al., 1999], the subduction of these volcanic highs strongly deforms the overriding plate margin and also influences the seismicity across the subduction interface and the magmatic activity of the volcanic arc [Nur and Ben-Avraham, 1981; *McGeary*, 1985; *Tatcher*, 1989]. Recent works propose that when these volcanic highs reach the seismogenic zone, they modify the seismic coupling and favor the nucleation of strong earthquakes [*Christensen and Lay*; 1988; *Cloos*, 1992; *Scholtz and Small*, 1997]. *Small and Abbott* [1998] even suggest that the subduction of very large seamounts (e.g., the Louisville ridge in the Tonga-Kermadec Trench) could fracture the surrounding oceanic crust.

Geophysical data recorded during oceanographic cruises allow detailed studies of the morphology and structure of convergent margins. Nevertheless, while seismic profiles succeed in resolving the geologic structure of the upper plate in relatively undeformed regions of a margin, interpretation becomes difficult when the subduction of a seamount occurs. In such areas the accretionary wedge and the frontal margin are so strongly deformed that the internal structure is poorly resolved.

Sandbox experiments already have been used to study sedimentary accretionary wedges and seamount subduction [*Davis et al.*, 1983; *Malavieille*, 1984; *Lallemand et al.*, 1992; *Kukowski et al.*, 1994; *Gutscher et al.*, 1998]. It appears from these studies that analog experiments afford good tools to complement the marine observations.

We have used similar sandbox experiments to investigate the structural evolution of the overriding plate margin in response to seamount subduction. We analyze structures in two and three dimensions, the evolution in time and space of the stress field induced by the seamount, and we estimate the amount of material transfer within the margin. The main purpose of this experimental study is to improve our understanding of the deformation mechanisms occurring during seamount subduction and to propose some quantitative results. Indeed, since fluids and pore pressure are not considered, angles of repose and angles of taper are greater than those observed in nature. Nevertheless, as demonstrated by morphologic comparisons between previous experiments and natural cases [*Dominguez et al.*, 1998], we believe that the mechanisms observed in such sandbox experiments are analog to those occurring in subduction zones.

Figure 2 summarizes the main morphologic features induced by seamount subduction, presented in previous works [*Dominguez et al.*, 1994, 1998]. The accretionary wedge is indented, and a large reentrant develop associated with a critical frontal slope, where massive sedimentary sliding

Paper number 1999TC900055
0278-7407/00/1999TC00055$12.00

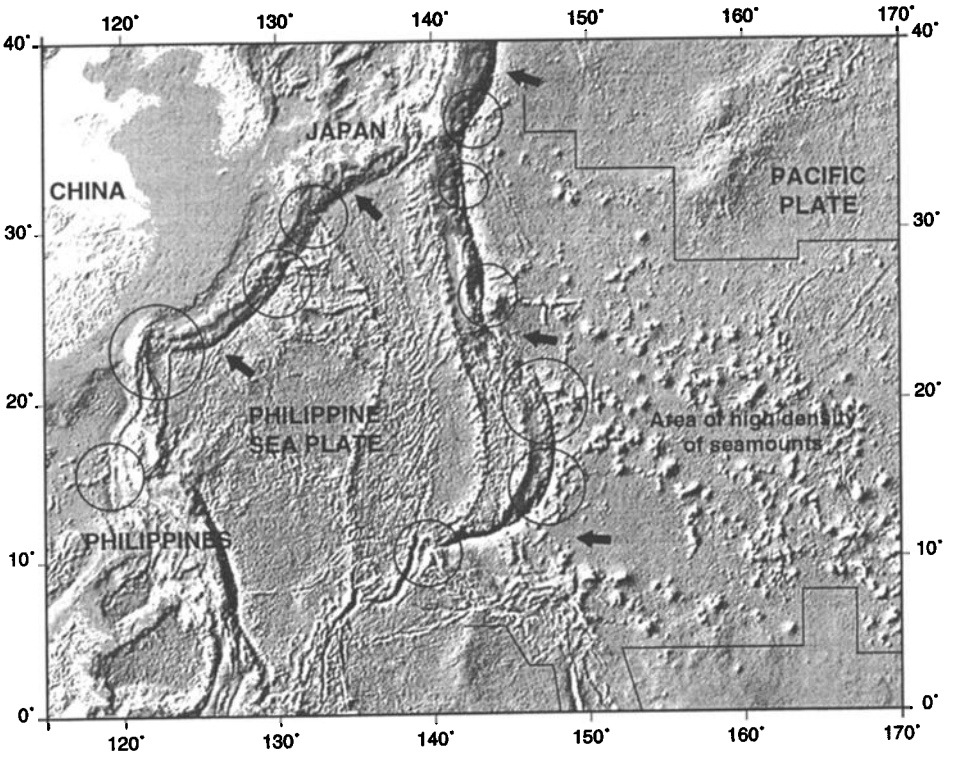

Figure 1. Shaded view of the Pacific and Philippine Plates showing the morphologic features of the seafloor. Areas of high density of seamounts are outlined as well as regions of seamount or ridge subduction (circles).

occurs. Landward of the reentrant, the margin is uplifted above the subducted seamount and shows a characteristic fault network. Seaward dipping back thrusts and conjugated strike-slip faults, related to the indentation of the margin, propagate landward as the seamount subduct.

1.2. Experimental Setup

The two experimental devices used to perform the sandbox experiments (Figure 2) are comparable to those used by *Malavieille et al.* [1991] and *Dominguez et al.* [1994; 1998]. Both consist of an inclined rigid plate on which a mylar sheet, simulating the subducting oceanic plate slides, is located. This sheet is pulled beneath a rigid backstop which represents the undeformable part of the overriding plate. A cohesive sand wedge is built in front of this backstop to simulate the more compacted inner part of the accretionary wedge and the more cohesive seaward termination of the overriding plate [*von Huene and Scholl*, 1991]. The oceanic sediments carried by the subducting plate are built by sprinkling horizontal layers of colored sand on the mylar film. The sand layers and backstop wedge are composed of granular material (sand and rock powder). The sand used in our experiments is well-sorted eolian quartz sand with a grain size of about 250 μm. Its physical properties (angle of internal friction ϕs of 30° and a very low cohesion) satisfy the Mohr-Coulomb criteria [*Dahlen*, 1984, 1990; *Dahlen and Suppe*, 1984]. They can be considered as good analogs of natural sedimentary rocks and marine sediments. The basal friction along the sand-mylar interface is intermediate (ϕb=20°). Scaling is such as 1 cm in the sandbox experiment is equivalent to 1 km in nature [*Lallemand et al.*, 1992]. The cohesion of the sand and the cohesion of the rock powder, used in our experiments, are 20 Pa and about 100 Pa, respectively, and scale to 2 and 10 MPa [*Gutscher et al.*, 1998]. These cohesion values are very close to values of unconsolidated marine sediments and lithified sedimentary rocks [*Hoshino et al.*, 1972].

The shape of the subducting high is conical with a slope of 20°. It consists of a rigid core covered by a 2 cm thick layer of cohesive rock powder with a thin (< 1 cm) sand cover, simulating a volcanoclastic cover. The friction along the interface between the rigid core and the cohesive layer is moderate to high (close to ϕb=25°).

The first device, used to study in cross sections the different stages of a seamount subduction, has two lateral glass panes. They allow the deformation to be observed in real time on both sides of the experiment. The second device, dedicated to the study of the margin structure in three dimensions, is very much larger to avoid boundary effects. On this apparatus the model can be impregnated with water at the end of the experiment to increase the sand cohesion and to cut vertical and also horizontal cross sections.

The results of three selected sandbox experiments are described in this paper. The first one shows in cross section

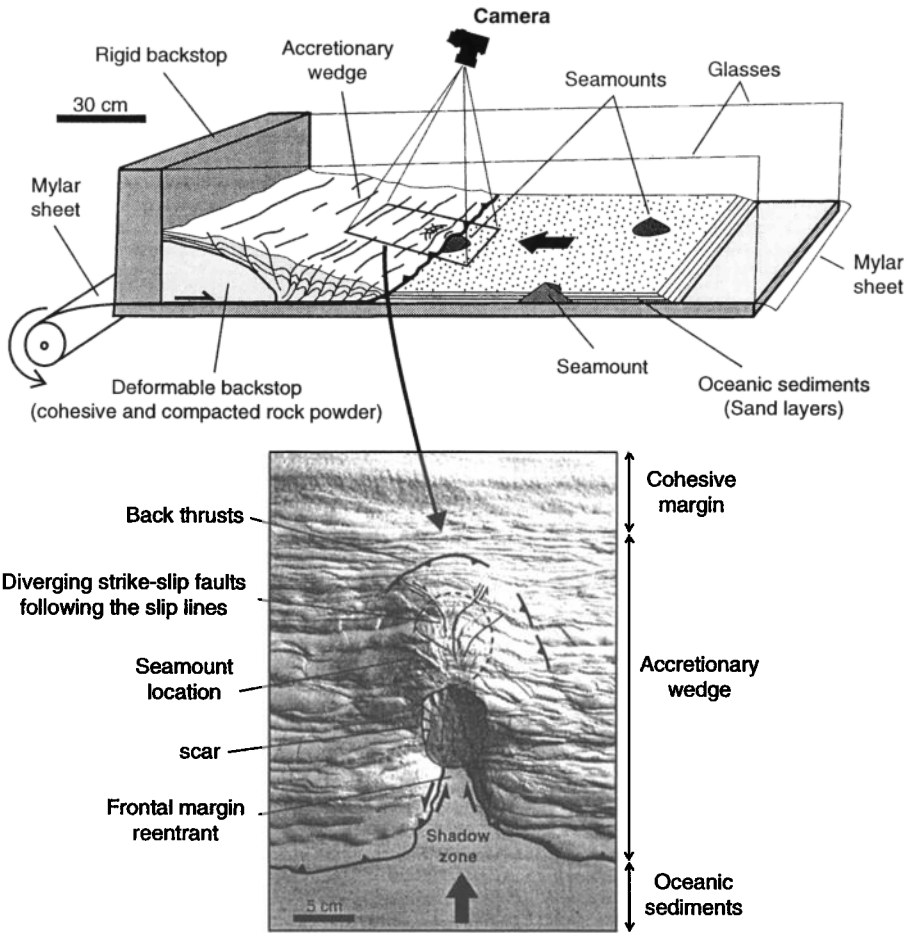

Figure 2. Principles of the experimental setup used to perform the sandbox experiments. Specific apparatus, based on the same principles, allow study of the deformation in two dimensions (cross section) or in three dimensions. The main morphotectonic features associated with the subduction of a conical seamount are summarized [see *Dominguez et al.*, 1998].

the progressive deformation of the margin during the subduction of a conical topographic high. The second presents horizontal cross sections performed in the accretionary wedge above the subducted high. The internal structure and deformations of the margin are then digitized and analyzed to determine the stress field around the subducted seamount. The third and final experiment concerns the subduction of three conical seamounts trending obliquely compared to the convergence vector. Vertical cross sections, parallel to the direction of the convergence, are used to estimate material transfer inside the deformed margin at three different stages.

2. Geometry, Kinematics, and Mechanics of Deformation Induced by Seamount Subduction

The deformational stages of seamount subduction are observed along a vertical cross section on the 2-D device. To study the section located directly above the top of the subducting seamount, a half cone is used. Lateral effects are not discussed in this 2-D experiment and will be studied in the next two experiments, using the 3-D device.

During the first 20 cm of convergence, an accretionary wedge develops by imbrication of frontal thrust slices against the cohesive wedge (Figure 3a). Some minor back thrusts, related to the growth of the accretionary wedge, slightly deform the front of the cohesive wedge.

2.1. First Stage: Uplift of the Frontal Margin

As the seamount starts to subduct, the frontal margin is uplifted. The basal décollement is deflected into the thin sand cover (analog to the volcanoclastic cover) of the seamount flank (Figure 3b). Part of this cover is locally off-scraped and accreted beneath the frontal thrust unit (Figure 4a). Because of the shape of the subducting high, the décollement slope abruptly changes to bypass the seamount. As a consequence, the frontal taper of the margin increases as well as the friction along the basal décollement, which now crosses through the seamount sand layer. The frontal part of the accretionary wedge deforms to reach the steeper critical slope that is

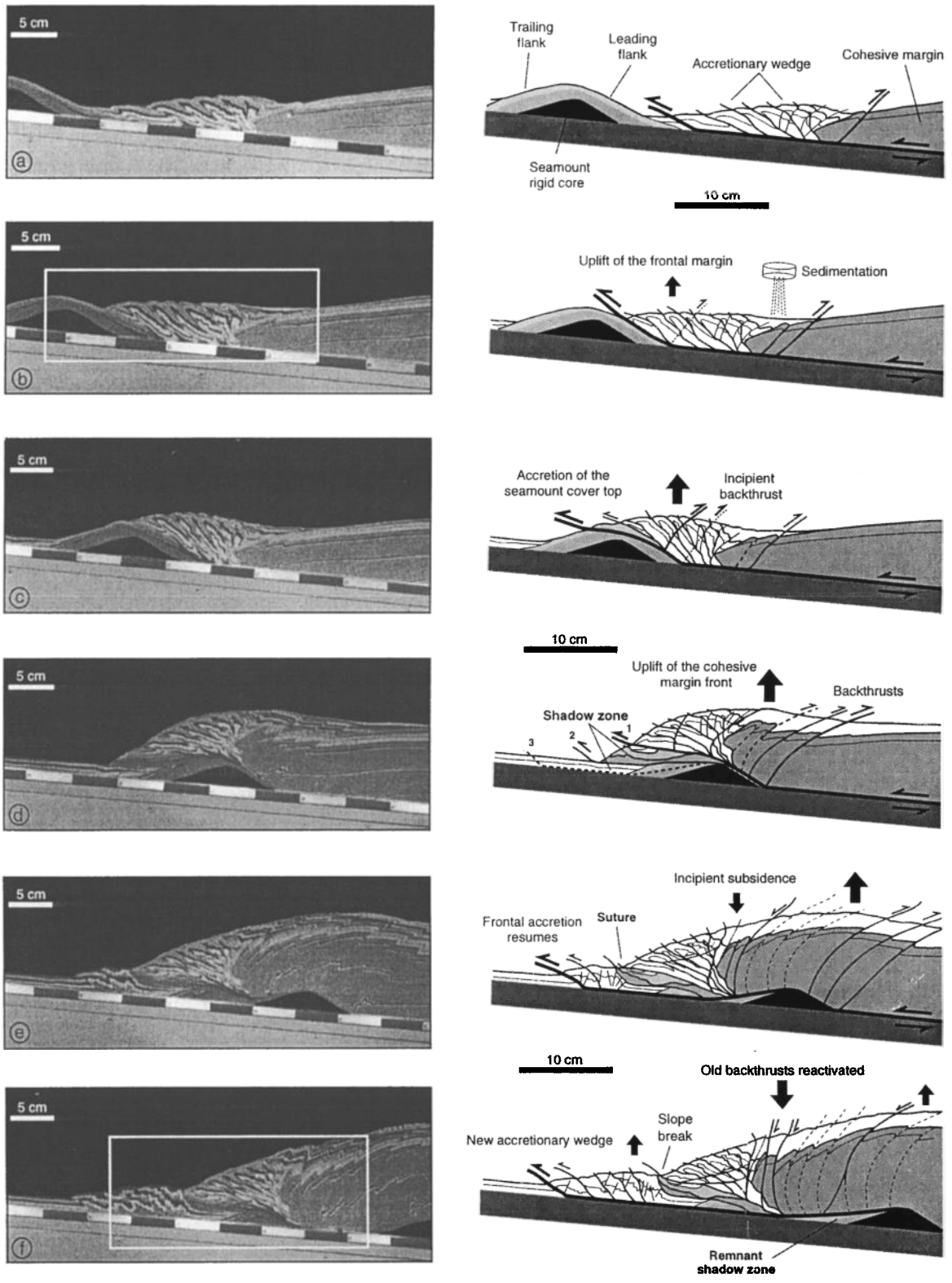

Figure 3. (a-f) Photographs and structural interpretation of the first experiment showing the different stages of conical seamount subduction in cross section. The experimental set-up consists of a glass-sided box so that the deformation can be observed in real time. The trenchfill (1.2 cm thick) consists of six layers of colored sand, and the seamount is composed of a rigid core covered by a cohesive layer of rock powder plus a thin sand cover. The cohesive sand wedge dips 5°, and its initial length is 65 cm. Black arrows show the relative vertical movements affecting the accretionary wedge during seamount subduction. The greatest part of the seamount cover is underplated just beneath the front of the margin.

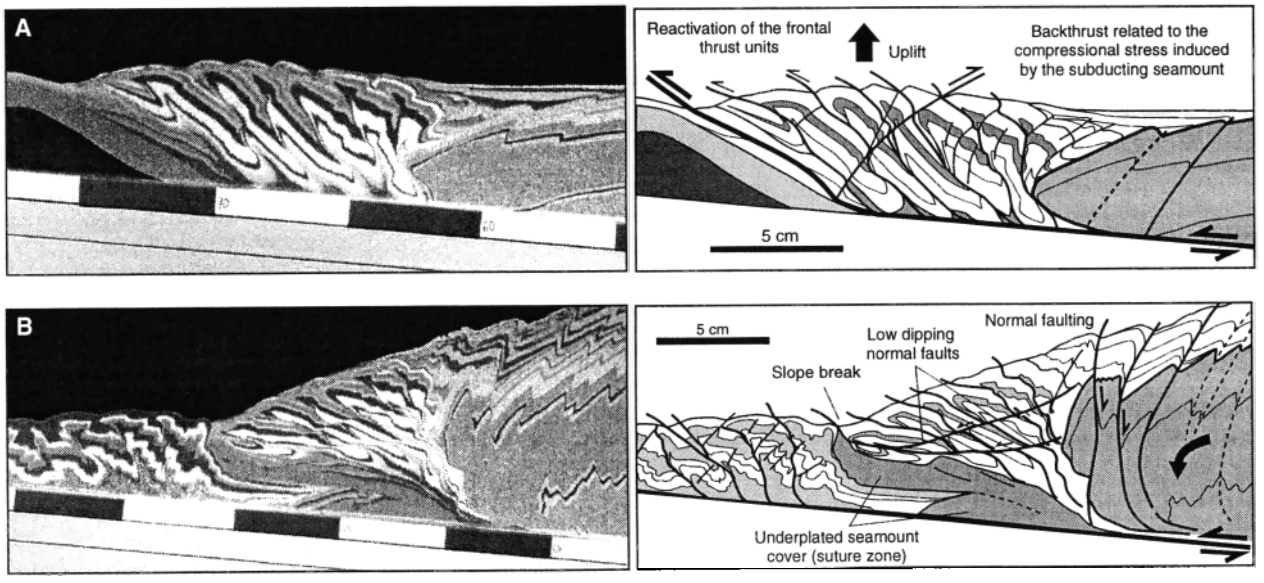

Figure 4. Enlargements of a conical topographic high showing details of margin deformation: (a) initial stage and (b) final stage.

associated with the new geometry and basal friction of this portion of the décollement. At this stage, reactivation of the thrusts is observed, inducing a general shearing of the accretionary wedge, coupled with a significant compaction (6% between Figure 3a and 3b). These mechanisms in the very early stages of subduction accommodate the shortening and thickening of the accretionary wedge. A ponded basin develops on the backside of the thickened wedge, which is filled with sediments (sand).

2.2. Second Stage: Indentation of the Accretionary Wedge

After 10 cm of seamount subduction, half of the topographic high is now buried beneath the accretionary wedge (Figure 3c). The top of the subducting seamount cover is off-scraped and accreted to the frontal margin. Because of the compressional stress induced by the subducting seamount, compaction of the accretionary wedge increases (5% between Figure 3b and 3c). Finally, when thrust reactivation and compaction have reached their limits, back thrusts initiate at the base of the subducted seamount slope and accommodate the uplift of the accretionary wedge and part of the convergence (Figure 4a). The basal décollement, located on the leading slope of the subducted seamount, still accommodates the greatest part of the convergence. At this stage the frontal margin records a rapid uplift correlated with the height of the subducting seamount.

2.3. Third Stage: Initiation of a Shadow Zone and Indentation of the Cohesive Margin

After 40 cm of convergence the seamount is completely subducted and starts uplifting the rear part of the accretionary wedge and the seaward end of the cohesive wedge (Figure 3d). As the seamount subducts beneath the margin, the load on its leading slope increases rapidly. The basal décollement jumps down to the interface between the rigid core and the cohesive layer at which friction is less. The cohesive layer of the seamount's leading slope is then accreted beneath the frontal margin, whereas its trailing slope remains relatively undeformed. The seamount subduction strongly disturbs the stress field, and the basal décollement is deflected upward in its wake. The décollement crops out in the middle part of the frontal slope margin, which develops an overcritical slope where sedimentary mass sliding is active. A large shadow zone forms in the wake of the seamount. The trenchfill sediments and part of the frontal margin are dragged into the subduction zone along with the seamount (Figure 3d).

After further convergence, the décollement jumps back down to the top of the subducting sedimentary sequence, in the wake of the seamount. Shearing of the material located in the shadow zone suggests that a small part of the convergence is still accommodated along the previous position of the décollement. Only the trenchfill sediments continue subducting in the wake of the seamount without significant deformation.

2.4. Fourth stage: Subsidence of the Frontal Margin

After 50 cm of convergence the seamount subducts beneath the cohesive margin. This cohesive part of the model simulates older accreted sediments and part of the deformable termination of the upper plate basement (Figure 3e). Reactivation of remnant back thrusts, as well as initiation of new ones generated by the seamount, is observed.

Because of the increasing load on the seamount's trailing slope and the increase of the friction surface between the shadow zone and the rest of the margin, a new basal décollement initiates at the base of the subducting trench fill sequence. Frontal accretion resumes, and a new accretionary wedge develops at the front of the margin.

During a certain amount of convergence both décollements are active, and an intense shearing of the margin material from

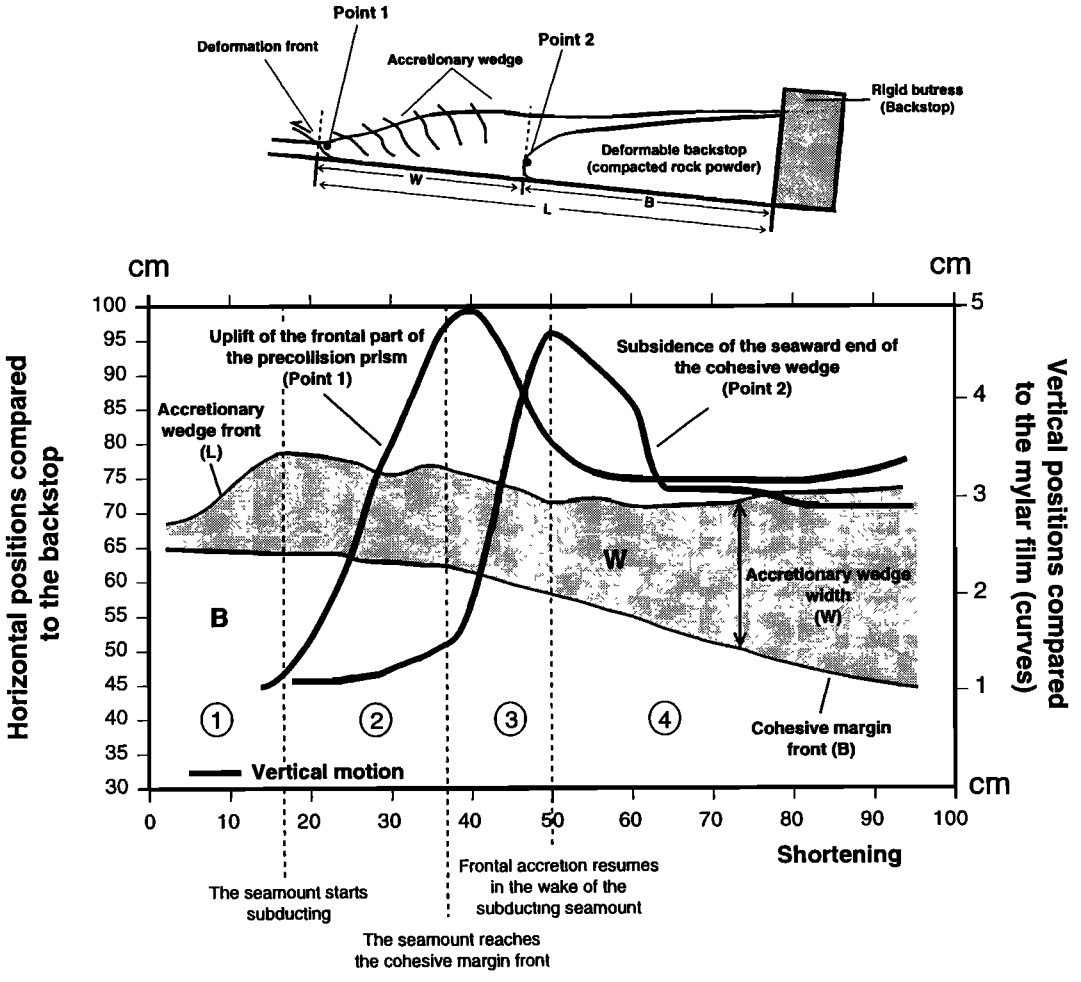

Figure 5. Diagram showing vertical and horizontal motion of the deformation front and the seaward end of the cohesive margin with respect to the rigid backstop. The different stages of retreat of the margin and the effects on the wedge growth induced by the seamount subduction are quantified by the two curves.

the shadow zone is observed. Finally, the upper décollement dies, and the basal décollement accommodates the whole convergence. As a consequence, the greatest part of the margin and trench fill sediments, dragged into the subduction zone behind the seamount, are underplated beneath the accretionary wedge. The size of the shadow zone reduces to approximately half of the seamount volume. The underplating of large volumes of sediment generates a rapid subsidence in the wake of the seamount, located beneath the rear part of the accretionary wedge (Figure 3e). The old back thrusts, now located above the seamount trailing slope are reactivated with a normal component. Conjugate normal faults dipping landward, and seaward dipping listric normal faults affecting the accretionary wedge are also observed (Figure 3e). At this stage the frontal slope exhibits a typical slope break (suture), which separates parts of the accretionary wedge developed before and after the seamount subduction.

2.5. Fifth Stage

After 60 cm of convergence the topographic high subducts beneath the cohesive part of the overriding plate (Figure 3f). A remnant shadow zone, composed mainly of part of the seamount cover and material scraped from the base of the cohesive margin, is still observed in the wake of the seamount (Figure 4b).

Other sandbox experiments, not presented in this study, show that the size of this remnant shadow zone depends on the friction along the basal décollement level (here along the mylar-sand interface). High basal friction favors the development of a much larger shadow zone, because there is no lower friction level at the base of the subducting sedimentary sequence. The décollement remains in an upper position much longer. The greatest part of the accretionary sequence is then definitively subducted or underplated beneath the cohesive part of the margin.

2.6. Kinematics

During the experiment the seaward end of the accretionary wedge (the deformation front) and the termination of the cohesive wedge are recorded with respect to the rigid backstop, as well as their vertical motions (Figure 5). The seaward growth of the accretionary wedge (Figure 5, stage 1)

occurs at a rate of about 0.75 cm/cc (where cc refers to centimeters of convergence). During this stage the cohesive margin front records only a very little landward displacement (a total of 1 cm) related to the initiation of minor back thrusts.

When the seamount starts subducting, frontal accretion ends, and the deformation front stops propagating seaward (Figure 5, stage 2). The back thrusts generated by the seamount induce a modest retreat of the accretionary wedge at a rate of about 0.1 cm/cc and a rapid uplift close to 0.2 cm/cc (Figure 4a). The subduction of the seamount strongly deforms the cohesive wedge. The shortening of this part of the margin accelerates to 0.3 cm/cc, and the wedge front records a retreat at the same rate (Figure 5, stage 3).

After 35 cm of seamount subduction (50 cm of convergence), frontal accretion resumes, and the seaward end of the cohesive margin starts to record a rapid subsidence (-0.05 cm/cc). The effects of the seamount on the evolution of the accretionary wedge structure progressively decrease (Figure 5, stage 4). The deformation front again propagates seaward but at a lower rate, because the shortening of the cohesive margin still continues (Figure 5, stage 1). After 80 cm of seamount subduction the total retreat of the cohesive margin front is close to 20 cm. At this stage the landward motion of the cohesive margin tends to decrease significantly, but the seamount still slightly disturbs the development of the accretionary wedge in its wake.

3. The 3-D Structure of the Margin in the Vicinity of a Subducted Seamount

This experiment is performed with experimental parameters comparable to the first 2-D experiment (Figures 6a and 6b). When the seamount is subducted beneath the accretionary wedge, the model is carefully impregnated with water to increase the sand cohesion (Figure 6c). This method permits cutting horizontal cross sections, showing the internal structure of the accretionary wedge around the subducted seamount (Figure 7).

3.1. Description of the Cross Sections

The first horizontal section cuts the circular bulge located above the seamount (Figure 8a). Minor out-of-sequence thrusts are observed in the cohesive part of the margin. They initiate during the first stages of the experiment and are associated with the growth of the accretionary wedge. Curved back thrusts generated by the seamount can also be observed above and landward of the subducted seamount position. At this stage they only affect the accretionary wedge, which is uplifted and thickened.

The second section is located just above the top of the subducting seamount (Figure 8b). The accretionary thrust units are clearly deformed. They curve landward in the vicinity of the seamount. Close to the subducting seamount, out-of-sequence thrusts affect the middle part of the accretionary wedge. They develop from above the top of the seamount and propagate seaward on each side. Laterally, they connect with the preexisting thrust units of the accretionary wedge. A large part of the frontal margin is thus underthrust beneath the rear part of the accretionary wedge. In the wake of the seamount a strongly deformed seaward dipping thrust unit is observed. It corresponds to the frontal part of the margin, indented during the first stage of the seamount subduction and now subsiding in the wake of the seamount.

The third section cuts the top of the subducting conical high (Figure 8c). The thrust units of the accretionary wedge located above the seamount's leading flank are strongly deformed and stretched. Some conjugate strike-slip faults with small offsets can be observed despite the intense crushing of

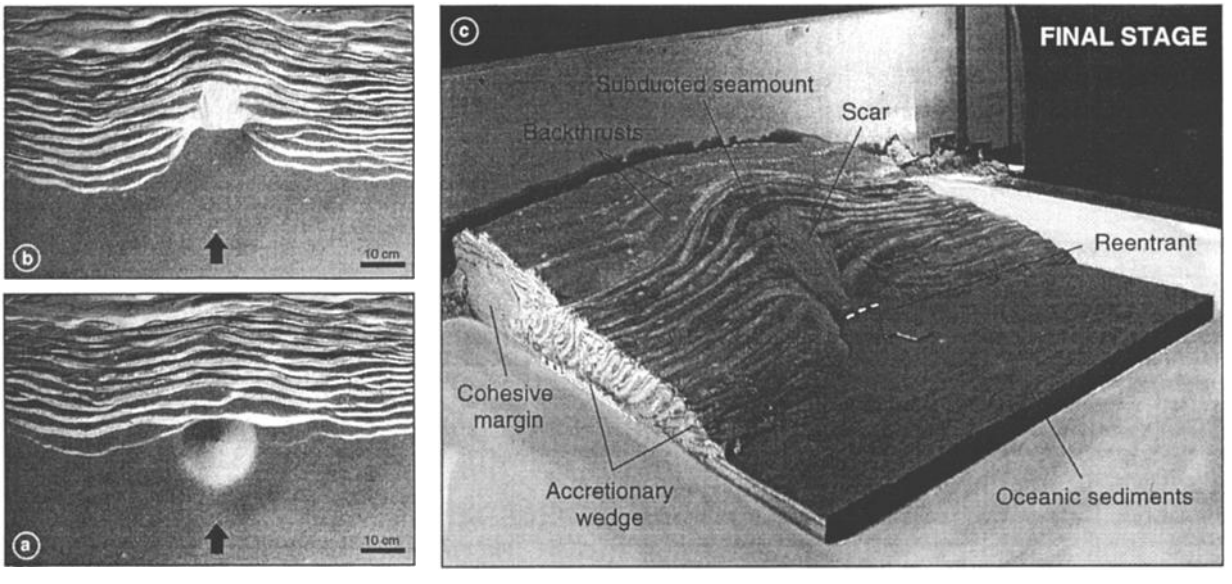

Figure 6. (a,b) Planar photographs of the second experiment. (c) A perspective view of the second experiment. When the topographic high is completely subducted beneath the accretionary wedge, the model is carefully impregnated with water to increase the sand cohesion. Sections are then cut to study the deformation of the wedge structure.

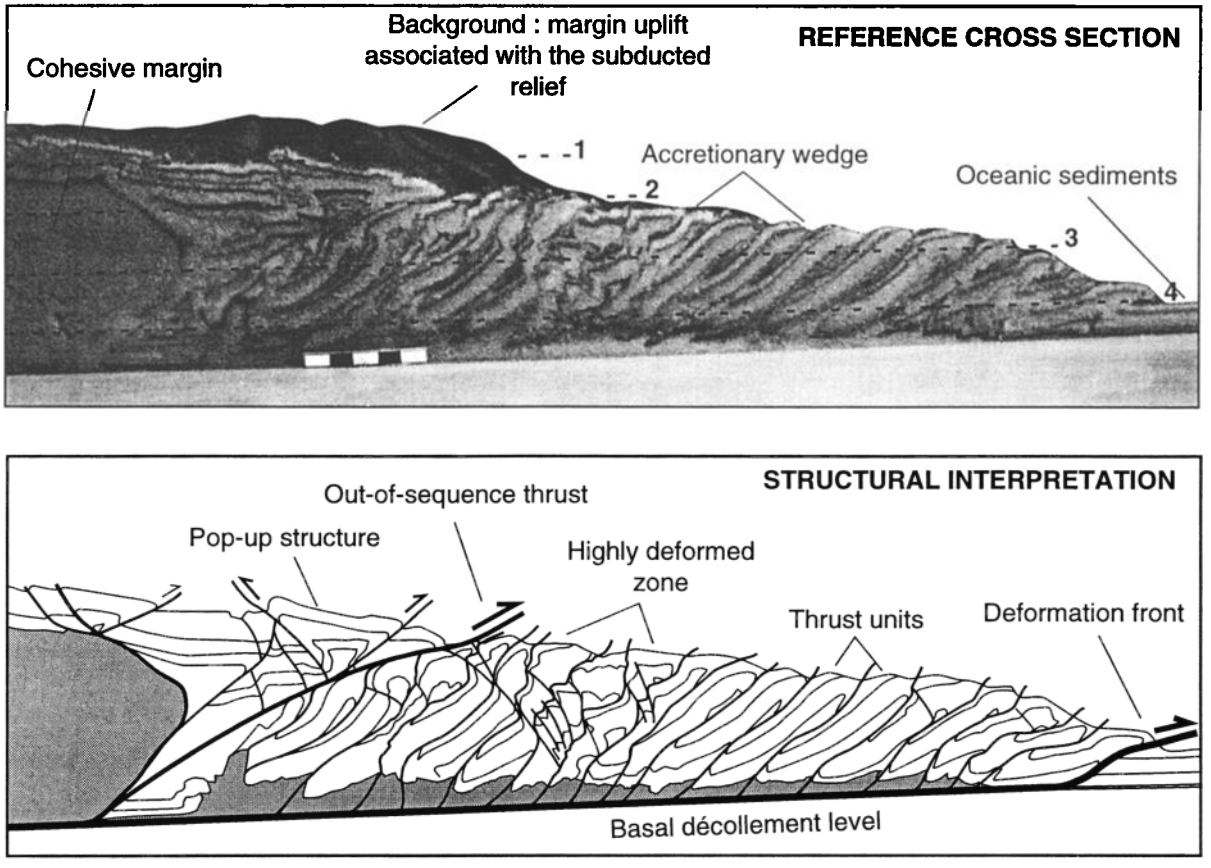

Figure 7. Photograph and structural interpretation of the reference section, trending parallel to the direction of convergence. These depictions show the structure of the accretionary wedge and the seaward end of the cohesive wedge in a region situated outside the deformation generated by the seamount. Dashed lines show the location of the horizontal cross sections presented.

the accretionary wedge in this area. Seaward of the seamount top, two faults trending parallel to the direction of convergence bound the upper part of the shadow zones which is located in the wake of the seamount.

The last cross section cuts the margin at the top of the subducting sedimentary sequence (Figure 8d). This section provides good constraints on the margin structure in the wake of the seamount and on the shape of the shadow zone.

Seaward of the subducting high, part of the seamount cover and the trenchfill sequence located in the shadow zone can be observed and appears to be undeformed. Two transfer zones, which connect to the base of the leading seamount flank, bound the shadow zone. These faults have a strike-slip component close to the trailing seamount flank. Farther seaward, they also exhibit a superimposed thrust component, which suggests that the shadow zone is progressively reduced in width. A reconstruction of the décollement surface geometry is shown in Figure 9. The main out-of-sequence plane is also represented.

The décollement molds the shadow zone in the wake of the seamount. At this stage the volume of the shadow zone is comparable to the size of the seamount if we consider the trench fill sediments located in the margin reentrant.

3.2. Stress Field Deduced From the Fault Network

We roughly estimated the shape of the global stress field around the subducted topographic high (Figure 10). This reconstruction is based on the interpretation of the previous horizontal cross sections, the study of the fault network, and morphologic studies (Figure 2 and *Dominguez et al* [1998]). Above the leading slope of the seamount the bending of the accretionary thrust units associated with curved back thrusts and conjugated strike-slip faults (better observed in the morphology) indicates that the major component of the stress field (σ_1) diverges landward. The indentation of the margin occurs above the leading slope of the seamount and does not extend far away on both sides. Laterally, the thrust units appear to abruptly strike normal to the direction of convergence.

Conjugate shear zones associated with strike-slip faults trending oblique to the direction of convergence suggest that σ_1 tends to converge in the wake of the seamount. Furthermore, subsidence and extension observed in this area confirm that σ_3 tends to parallel the relative plate motion in the wake of the seamount. Finally, the successive shapes of the deformation front during closing of the reentrant when

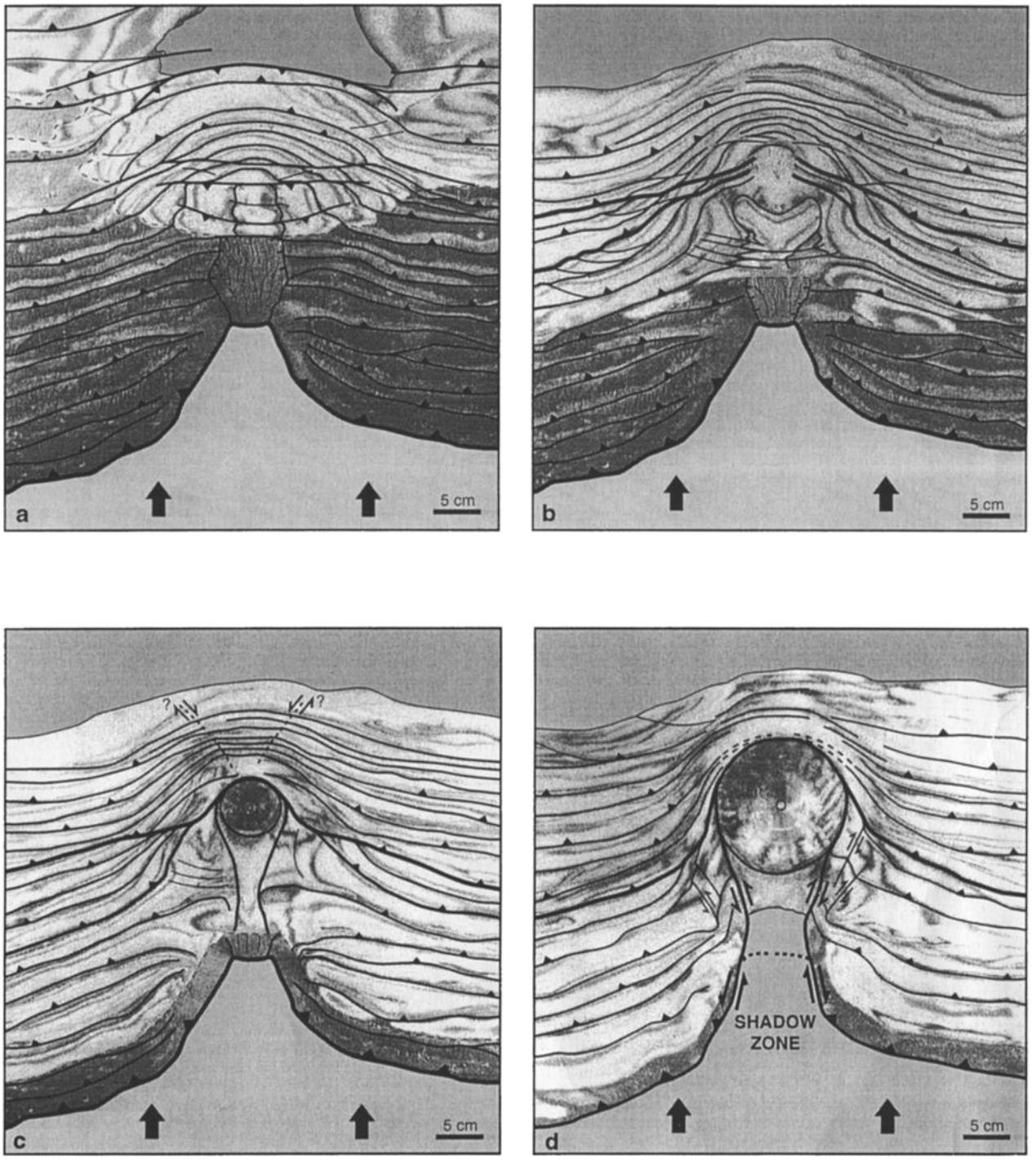

Figure 8. (a-d) Photographs of the horizontal cross sections discussed in the text.

frontal accretion resumes indicates that σ_1 becomes increasingly parallel to the convergence.

4. Deformation and Material Transfer Within the Accretionary Wedge

The subduction of three conical topographic highs, trending obliquely with respect to the direction of convergence, is performed to study material transfer inside the margin at three different stages of seamount subduction. At the end of the experiment the model is impregnated with water, as for the second experiment, and cut by 30 vertical cross sections, all parallel to the direction of convergence (Figure 11).

4.1. Description of the Cross Sections

A reference cross section is cut far from the effect of seamount subduction and shows the structure of the normal

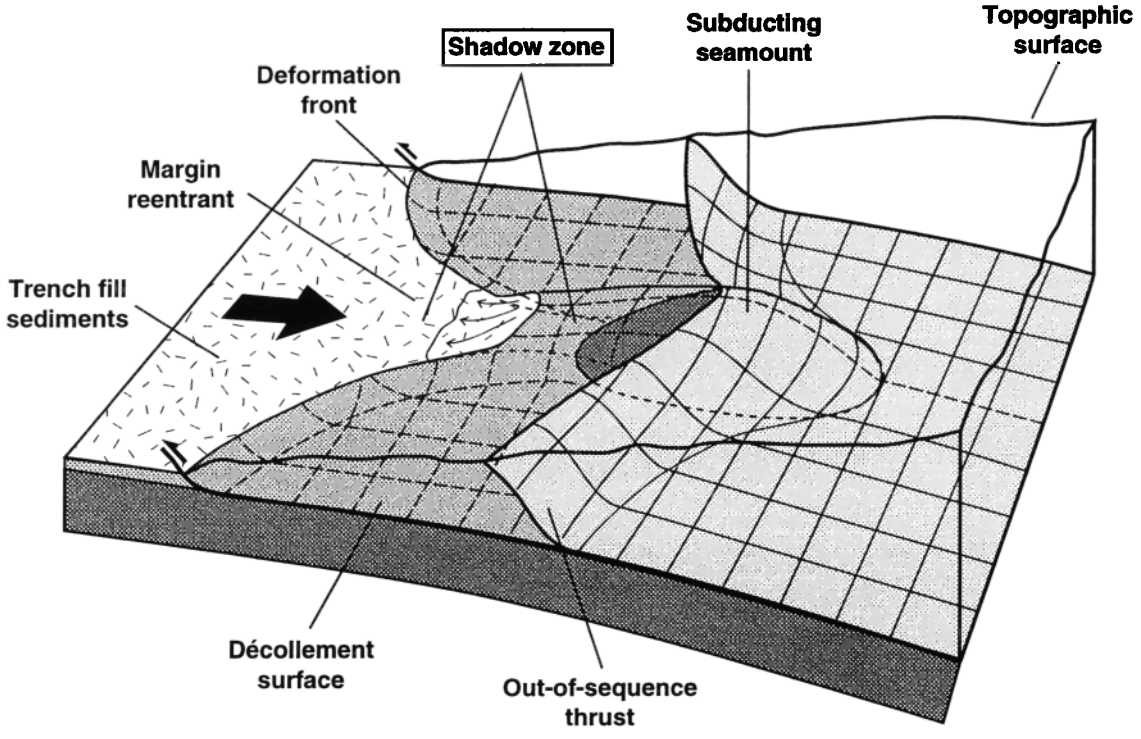

Figure 9. Block diagram showing 3-D geometry of the main thrust surfaces (décollement, shadow zone, and out-of-sequence thrust).

accretionary wedge (Figure 11. See reference cross section). Back thrusting of the rear part of the accretionary wedge onto the cohesive margin generates an "outer arc high" trending parallel to the backstop. It bounds a narrow morphological trough corresponding to the forearc basin, which is filled with sediment (sand) during the experiment.

Section A shows the structure of the margin above seamount 1, which is in the first stages of subduction and uplifts the frontal margin (Figure 11, section A). The basal décollement is deflected upward and emerges at the surface in the middle part of the frontal margin. Above the seamount trailing slope, a small shadow zone develops, mainly composed of parts of the seamount cover and some frontal margin sediments.

Section B shows the margin structure above seamount 2 buried at the boundary between the accretionary wedge and the most compacted part of the margin (Figure 11, section B). At this stage, frontal accretion has already resumed, and a new accretionary wedge develops. A volume of frontal margin material, comparable to the size of the subducting high, is underplated beneath the rear part of the wedge. As a consequence, the accretionary wedge exhibits a steep slope (19°) in this area, whereas the frontal slope dips only 5°. The slope break marks the suture zone.

Section C is located through the seamount 3, which is deeply buried beneath the cohesive wedge (Figure 11, section C). Here the effects of seamount subduction on the margin structure are most important.

In the middle part of the accretionary wedge, near the suture area, the lower parts of the thrust units are missing. A very

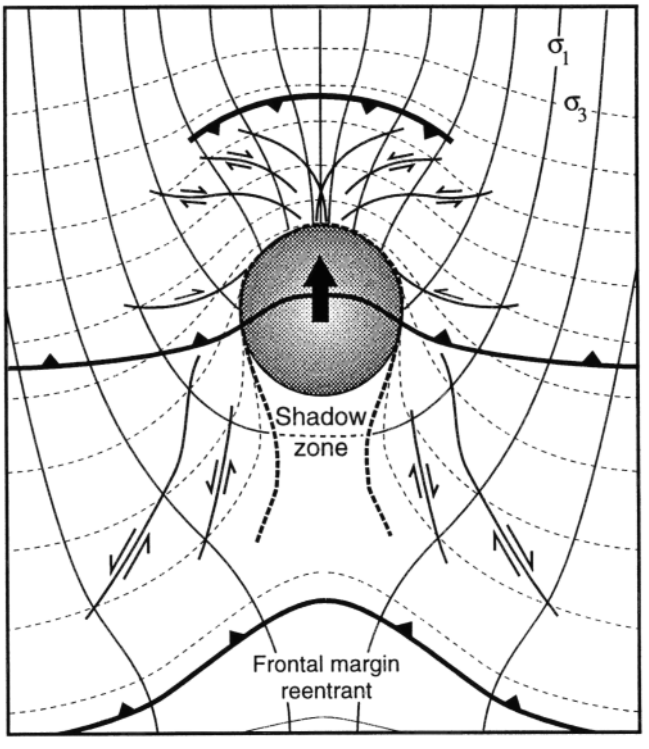

Figure 10. Shape of the stress field around the subducted seamount. The main thrusts and fault network, deduced from the experiments presented and previous morphological studies are superimposed.

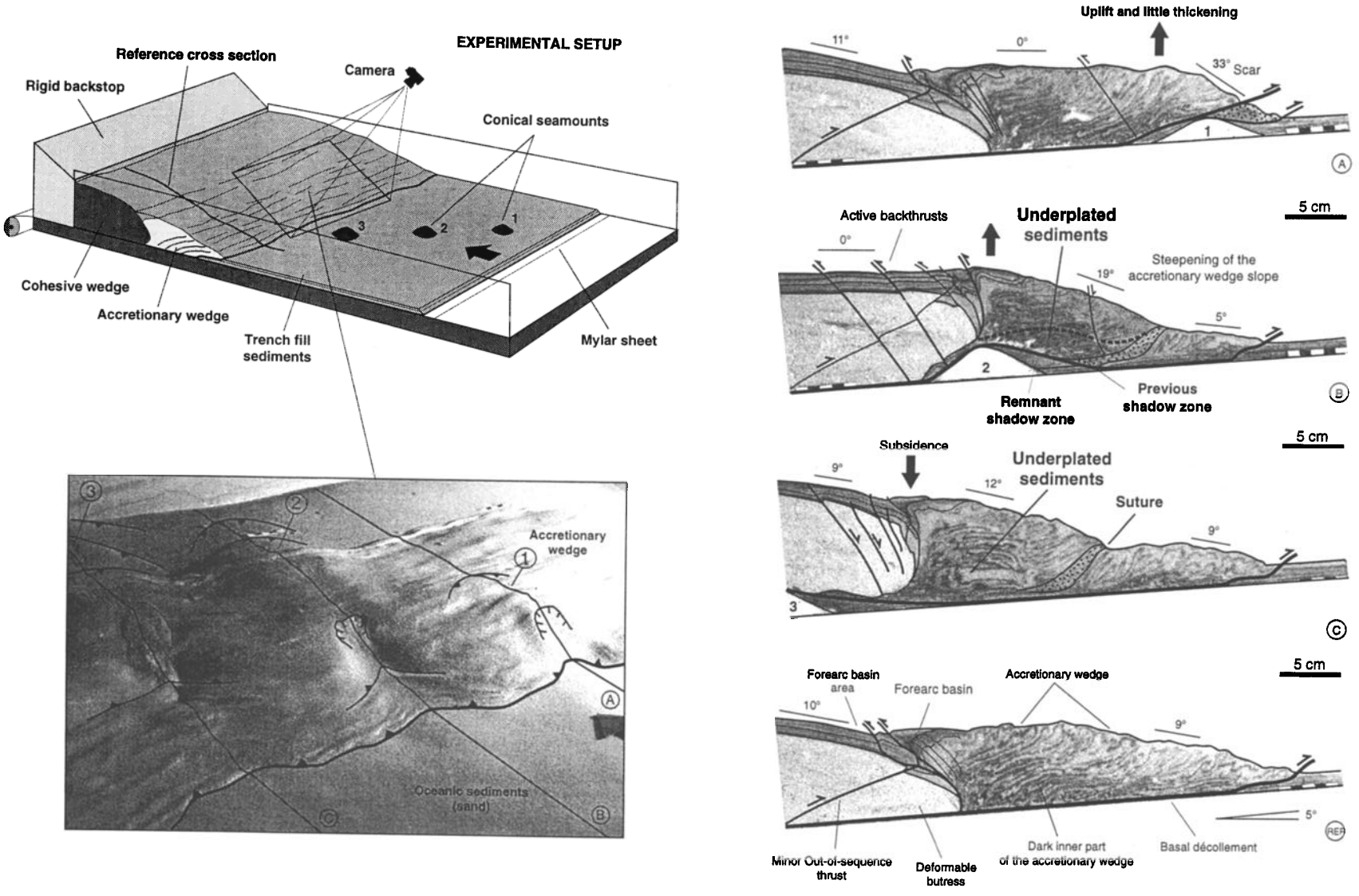

Figure 11. Experimental setup of the third experiment showing the 3-D device and the position of the reference cross section. We cut 30 sections parallel to the convergence to reconstruct the structure of the accretionary wedge. Locate the three interpreted cross sections, situated straight across the subducted seamounts. They reveal the material transfer inside the margin at three stages of seamount subduction.

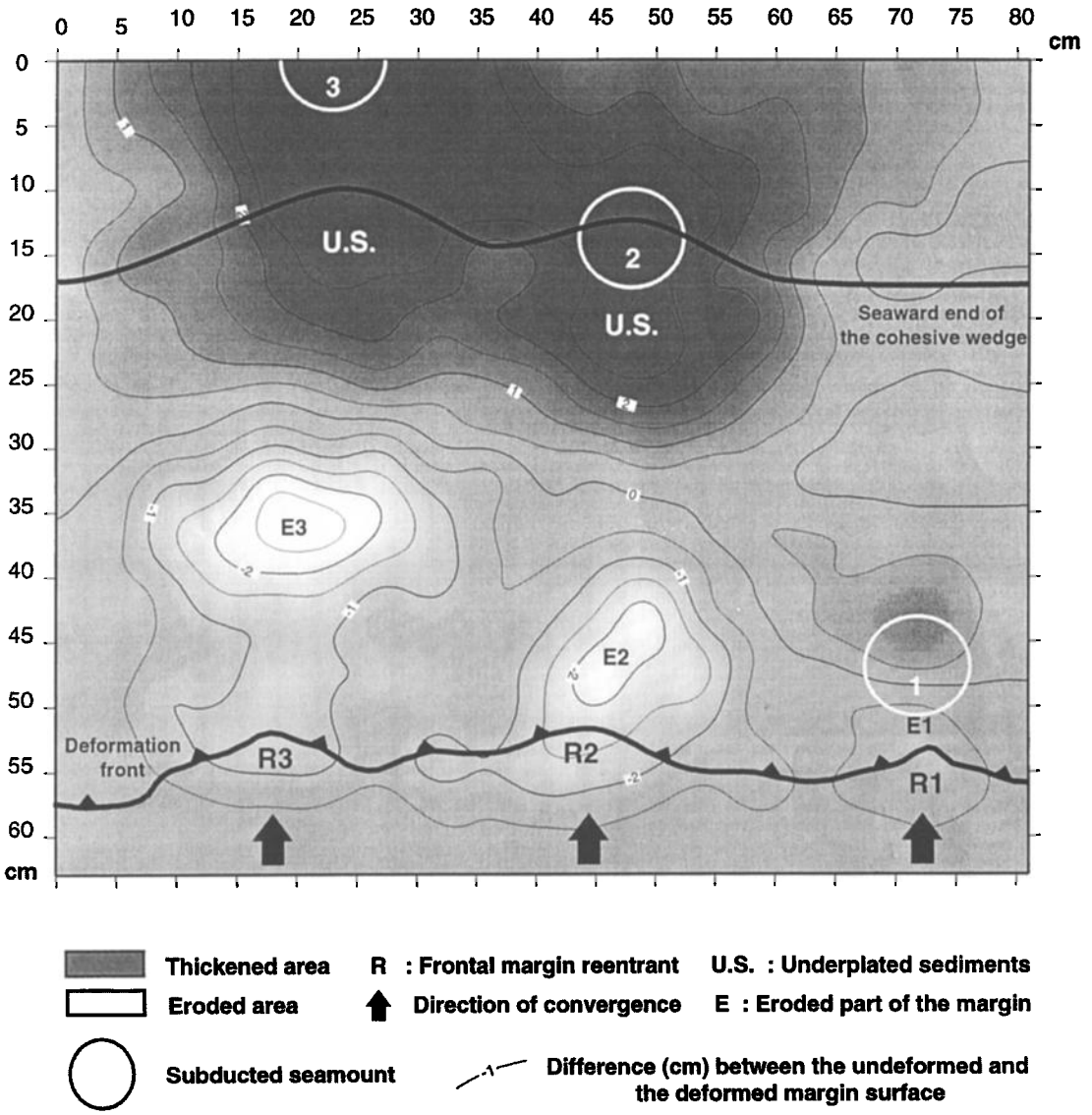

Figure 12. Map illustrating the transfer and underplating of frontal margin material to the rear part of the margin. Dark shading with positive contours corresponds to the region thickened at the end of the experiment. Light shading and white areas with negative contours correspond to regions of the margin eroded during the seamout subductions.

long underplated unit is observed instead, which corresponds to the part of the trench fill sequence previously dragged into the subduction zone behind the seamount. In this region the lower part of the accretionary wedge is strongly eroded and has been transported into the seamount shadow zone and finally underplated landward.

Part of the accretionary wedge sediments appears to subduct with the seamount beneath the cohesive wedge in a reduced shadow zone. The intense deformation of the sediments located in this remnant shadow zone suggests internal shearing induced by a vertical velocity gradient inside this kind of subduction channel. At this stage the amount of material dragged into subduction appears to be greatly reduced (about half of the seamount volume) compared to the size of the shadow zone when the seamount was subducting beneath the accretionary wedge.

4.2. Material Transfer in Three Dimensions

The 30 cross sections are processed to reconstruct the 3-D structure of the margin and to calculate the material transfer (Figure 12). The topography of the deformed margin is digitized using the vertical cross sections. The reference cross section is used to reconstruct, by interpolation, an undeformed margin topography at the same stage of convergence. Figure 12 shows in map projection the difference (calculated in centimeters) between the deformed and undeformed surfaces of the margin. Assuming that the

margin material cannot cross the rigid backstop (no output), the topographic differences between these two surfaces are directly linked to material transfer inside the margin. To avoid artifacts induced by the seamount shapes, the topographic effects of the seamount have been removed from the deformed topographic surface.

The negative contours (light shading and white areas in Figure 12) show the region of the margin where a material deficit exists (sediment has been removed), and the positive contours (dark shading in Figure 12) show the region of the margin where a material surplus exists (sediment has been added).

Seamount 1, which is the first stage of subduction, slightly deforms the frontal margin. A small thickened region (1 cm) located above the seamount's leading edge is observed. It corresponds to shortening associated with the reactivation of the accretionary thrust units.

Seamount 2 is more deeply subducted and has strongly disturbed the accretionary wedge in its wake. The frontal margin appears to be eroded over a large area, about 3 times larger than the seamount's basal surface. The amount of eroded sediment is estimated to be twice the seamount volume and is also comparable to the volume of excess sediment observed directly seaward of the seamount position. This thickened area, which extends laterally over more than 20 cm, reveals that the material previously eroded from the frontal margin is now underplated at the boundary between the accretionary wedge and the cohesive margin front.

A thickened area can also be observed above the seamount leading slope. It corresponds to the active deformation of the seaward end of the cohesive margin which records shortening.

Seamount 3 shows similar features. Nevertheless, because it represents a more advanced stage of deformation, some differences are observed. The deformation front is still slightly indented, but its morphology is nearly normal, because frontal accretion has resumed and a new accretionary wedge has developed. The eroded area of the margin is still observable and can be compared in size and volume to the one associated with seamount 2. The cohesive margin front is strongly indented, and the underplated sediment proceeding from the frontal margin lodges in this area. The volume of the margin affected by underplating of material and thickening of the cohesive margin appears to be very large (about 8 to 10 times the seamount volume). This last observation leads to the conclusion that the seamount subduction deforms the margin not only along its track but also regionally.

5. Discussion and Conclusion

The use of analog modeling can make a great contribution toward understanding the evolution of the deformation and quantifying the resultant material transfer. The sandbox

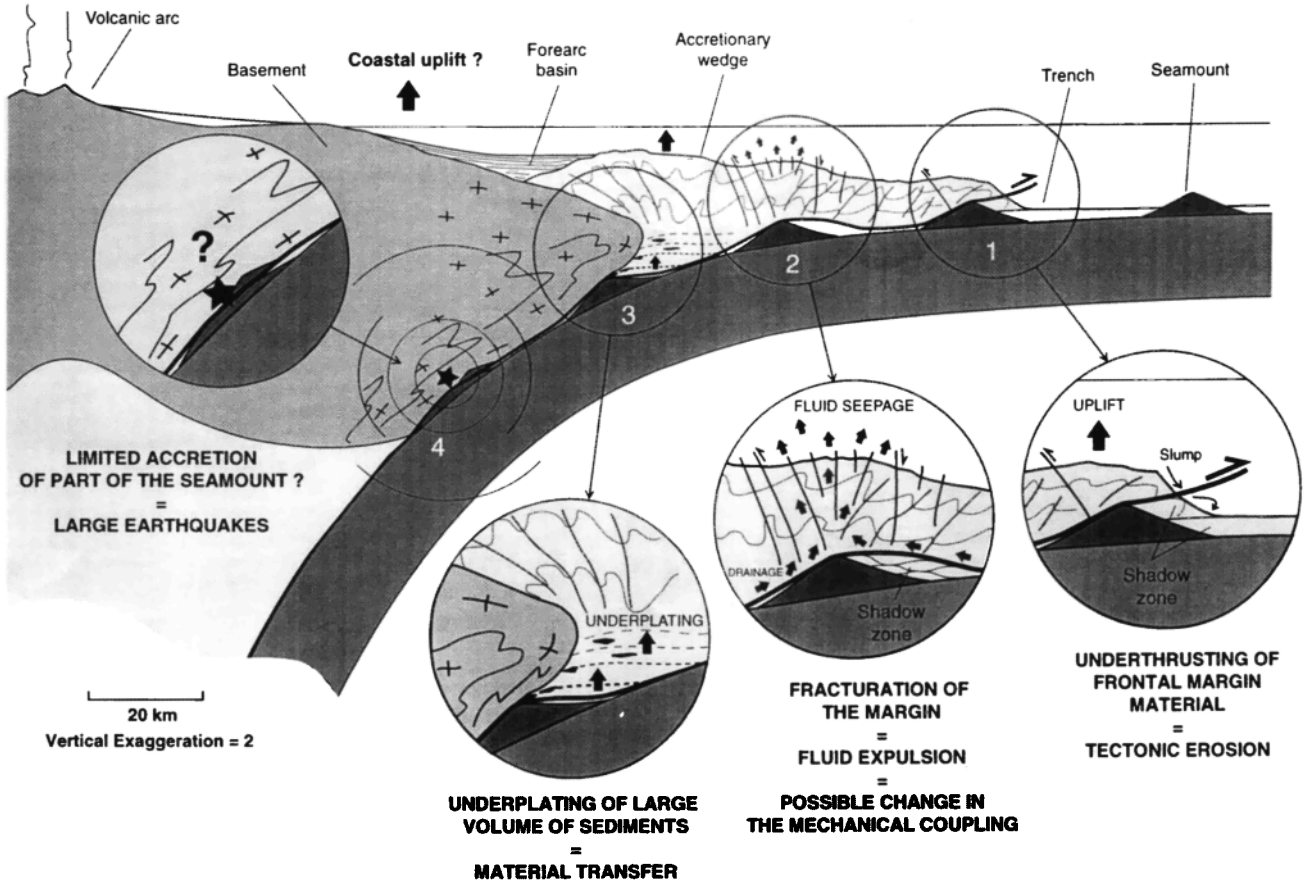

Figure 13. Schematic cross section illustrating material transfers inside the accretionary wedge induced by seamount subduction.

experiments described here show that the topographic highs carried by the subducting plate strongly interact with the growth of the accretionary wedge and greatly influence the tectonic regime of the margin (Figure 13).

Material transfer is expressed by different tectonic processes depending on the part of the margin being affected by the subducting high. The accretionary wedge and the inner compacted part of the margin undergo significant deformation including frontal margin erosion, removal and underplating of large volumes of sediment, indentation, and basal erosion of the cohesive part of the margin (Figure 13).

Regions of active margins where large oceanic crust features are subducting, such as Costa Rica [*Gardner et al.*, 1992; *Hinz et al.*, 1996; *Fisher et al.*, 1998] and the Tonga-Kermadec Trench [*Ye et al.*, 1996; *Ballance et al.*, 1989], show an intense tectonic erosion. If the mechanisms responsible for the deformation in our experiments are similar to those occurring at active convergent margins, seamount subduction appears to be responsible for an important part of the tectonic erosion observed in natural settings. We suggest that in such regions, seamount subduction is the main tectonic process controlling the geodynamic evolution of the whole margin and should be taken into consideration when calculating sedimentary mass balance.

Sandbox experiments reveal that the volume of sediments transfered from the frontal margin to the rear part of the accretionary wedge could be as much as 2 or 3 times the volume of the subducting highs. Some materials from the accretionary wedge are also removed and deeply buried beneath the more resistant part of the overriding plate margin.

Unfortunately, this estimation is only approximate since we do not consider the effects of fluids in our experiments, which necessarily limits an accurate quantification of the slope angles and material volumes. It is important to note, however, that our experiments clearly show that basal friction and margin rheology can significantly modify the evolution of the shadow zone during seamount subduction.

On the basis of the observations reported in this paper, we propose that the underplating of large volumes of relatively undeformed, water-laden sediments beneath the rear part of the margin could result in local variation of pore fluid pressure in the wake of the seamount. The dense fracture network generated by seamount subduction would favor fluid expulsion and induce a decrease in the fluid pressure and effective basal friction. It is possible, then, that such a mechanism contributes to regional variation of the mechanical and seismic coupling around subducting asperity.

Acknowledgments. The authors wish to thank C Small and Z. Ben-Avraham for their constructive comments that improved the manuscript The authors are grateful to M. Jolivet, B. Sanche, C. Y Lu, and A Deschamps for their help in performing the sandbox experiments and for technical support. M. A. Gutscher, G. W. Moore and P. Connolly are greatly acknowledged for grammatical corrections of the manuscript. Some figures presented in this paper have been done using GMT software [*Wessel and Smith*, 1991].

References

Ballance, P, D W Scholl, T L. Vallier, A.J Stevenson, H. Ryan, and R.H. Herzer, Subduction of a Late Cretaceous seamount of the Louisville Ridge at the Tonga Trench: A model of normal and accelerated tectonic erosion, *Tectonics*, *8*, 953-962, 1989

Batiza, R, Abundances, distribution and sizes of volcanoes in the Pacific Ocean and implications for the origin of non-hotspot volcanoes, *Earth Planet. Sci. Lett.*, *60*, 195-206, 1982

Christensen, D H., and T Lay, Large earthquakes in the Tonga region associated with subduction of the Louisville Ridge, *J Geophys. Res*, *93*, 13,367-13,389, 1988

Cloos, M., Thrust type subduction zone earthquake and seamount asperities· A model for seismic rupture, *Geology*, *20*, 601-604, 1992

Collot, J.Y, and M.A Fisher, Formation of forearc basins by collision between seamounts and accretionary wedges. An example from the New Hebrides subduction zone, *Geology*, *17*, 930-933, 1989.

Collot, J Y., and M Fisher, The collision zone between the North d'Entrecasteaux Ridge and the New Hebrides Island Arc, *J. Geophys Res.*, *96*, 4457-4478, 1991

Dahlen, F A, Noncohesive critical Coulomb wedges An exact solution, *J. Geophys. Res*, *89*, 10,125-10,133, 1984

Dahlen, F A., Critical taper model of fold-and-thrust belts and accretionary wedges, *Ann Rev Earth Planet. Sci.*, *18*, 55-99, 1990.

Dahlen, F A., and J. Suppe, Mechanics of fold-and-thrust belts and accretionary wedges· Cohesive Coulomb theory, *J. Geophys. Res.*, 89, 10,087-10,101, 1984.

Davis, D., J. Suppe and F A. Dahlen, Mechanics of fold-and-thrust belts and accretionary wedges, *J. Geophys. Res.*, *88*, 1153-1172, 1983.

Dominguez, S, S E Lallemand and J. Malavieille, New results from sandbox modeling of seamount subduction and possible applications, *Eos Trans AGU*, *75*, 671, 1994

Dominguez, S, S.E. Lallemand, J Malavieille, and R von Huene, Upper plate deformations associated with seamount subduction, *Tectonophysics*, *293*, 207-224, 1998.

Dominguez S., S. Lallemand, and J Malavieille, The oblique subduction of the Gagua Ridge beneath the Ryukyu accretionary wedge system, *Mar. Geophys Res*, in press, 1999

Fisher, M A., J.Y Collot, and E.L Geist, Structure of the collision zone between Bougainville Guyot and the accretionary wedge of the New Hebrides Island Arc, southwest Pacific, *Tectonics*, *10*, 887-903, 1991.

Fisher, D M., T W Gardner, J S Marshall, P.B Sak, and M. Protti, Effect of subducting sea-floor roughness on fore-arc kinematics, Pacific coast, Costa-Rica, *Geology*, *26*, 467-470, 1998

Gardner, T, et al, Quaternary uplift astride the aseismic Cocos Ridge, Pacific coast of Costa Rica, *Geol Soc Am Bull.*, *104*, 219-232, 1992.

Gutscher, M.A., N Kukowski, J. Malavieille, and S Lallemand, Material transfer in accretionary wedges from analysis of a systematic series of analog experiments, *J. Struct. Geol*, *20*, 407-416, 1998.

Hinz, K, R von Huene, and C R. Ranero, Tectonic structure of the convergent Pacific margin offshore Costa-Rica from multichannel seismic reflection data, *Tectonics*, *15*, 54-66, 1996

Hoshino, K., H. Koide, K Inami, S Iwamura, and S. Mitsui, Mechanical properties of Japanese Tertiary sedimentary rocks under high confining pressures, *Rep. 244*, 200 pp., *Geol Surv of Jpn*, Kawasaki, Japan, 1972

Kukowski, N, R. von Huene, J. Malavieille, and S Lallemand, Sediment accretion against a buttress beneath the Peruvian continental margin at 12°S as simulated with sandbox modeling, *Geol Rundsch*, *83*, 822-831, 1994

Lallemand, S E., J Y Collot, B Pelletier, C Rangin, and J P., Cadet, Impact of oceanic asperities on the tectogenesis of modern convergent margins, *Oceanol Acta*, *10*, 17-30, 1990

Lallemand, S.E., J. Malavieille and S Calassou, Effects of oceanic ridge subduction on accretionary wedges· Experimental modeling and marine observations, *Tectonics*, *11*, 1301-1313, 1992.

Malavieille, J., Modélisation expérimentale des chevauchements imbriqués. Application aux chaînes de montagnes, *Bull Soc. Géol. Fr*, *7*, 129-138, 1984.

Malavieille, J, C. Larroque, S E Lallemand and J F. Stephan, Experimental modelling of accretionary wedges, *Terra Nova Abstr.*, *3*, 367, 1991

McGeary, S, A. Nur, and Z Ben-Avraham, Spatial gaps in arc volcanism The effect of collision or subduction of oceanic plateaus, *Tectonophysics*, *119*, 195-221, 1985

Moore, G.F, and K L. Sender, Fracture zone collision along the south Panama margin, *Geol Soc Am., Spec Pap*, *295*, 201-212, 1995

Nur, A, and Z Ben-Avraham, Volcanic gaps and the consumption of aseismic ridges in South America, *Mem. Geol Soc. Am*, *154*, 729-740, 1981

Park, J O, T. Tsuru, Y Kaneda, Y Kono, S Kodaira, N. Takahashi and H. Kinoshita, A subducting seamount beneath the Nankai accretionary prism off Shikoku, southwestern Japan, *Geophys Res. Lett.*, *26*, 931-934, 1999

Scholtz, C.H., and C. Small, The effect of seamount subduction on seismic coupling, *Geology*, *25*, 487-490, 1997

Small, C and D. Abbott, Subduction obstruction and the crack-up of the Pacific plate ?, *Geology*, *26*, 795-798, 1998.

Smith, D K. and T.H. Jordan, Seamount statistics in the Pacific Ocean, *J Geophys Res*, *93*, 2899-2918, 1988

Tatcher, W., Earthquake recurrence and risk assessment in circum-Pacific seismic gaps, *Nature*, *341*, 432-434, 1989

von Huene, R., and D.W., Scholl, Observations at convergent margins concerning sediment subduction, subduction erosion, and the growth of continental crust, *Rev Geophys*, *29*, 279-316, 1991.

von Huene, R., et al, Morphotectonics of the Pacific convergent margin of Costa Rica, in *Geologic and Tectonic Development of the Caribbean Plate Boundary in Southern Central America*, edited by P Mann, *Spec. Pap. Geol. Soc. Am.*, *295*, 291-308, 1995

Wessel, P., and S. Lyons, Distribution of large Pacific seamounts from Geosat/ERS-1. Implications for the history of intraplate volcanism, *J. Geophys. Res*, *102*, 22,459-22,475, 1997

Wessel, P., and W.H.F Smith, Free software helps map and display data, *Eos Trans. AGU*, 72 441, 1991.

Ye, S., J. Bialas, E.R. Flueh, A. Stavenhagen, and Huene, R., 1996. Crustal structure of the Middle American Trench off Costa-Rica from wide-angle seismic data, *Tectonics*, *15*, 1006-1021.

S. Dominguez, S. Lallemand, and J. Malavieille, Laboratoire de Géophysique, Tectonique et Sédimentologie, ISTEEM, UMR 5573, CNRS, Université de Montpellier II, c.c 060, 34095 Montpellier, France. (stephdom@dstu.univ-montp2 fr)

(Received December 9, 1998;
revised May 17, 1999;
accepted July 29, 1999.)